



A novel efficient broadband model to derive daily surface solar Ultraviolet radiation (0.280–0.400 μm)

Wenmin Qin ^a, Lunche Wang ^{a,*}, Jing Wei ^{b,c}, Bo Hu ^d, Xun Liang ^a

^a Hunan Key Laboratory of Remote Sensing of Ecological environment in Dongting Lake Area, School of Geography and Information Engineering, China University of Geosciences, Wuhan, China

^b State Key Laboratory of Remote Sensing Science, College of Global Change and Earth System Science, Beijing Normal University, Beijing, China

^c Department of Atmospheric and Oceanic Science, Earth System Science Interdisciplinary Center, University of Maryland, College Park, MD, USA

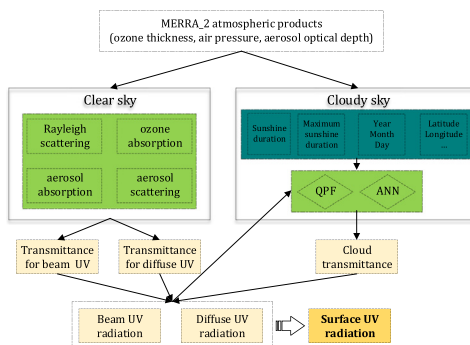
^d Institute of Atmospheric Physics, Chinese Academy of Sciences, Beijing, China



HIGHLIGHTS

- A model for calculating broadband surface solar UV radiation is proposed.
- This model has been evaluated in various climate zones over mainland China.
- The model was packaged into a software to facilitate the users.
- The spatial and temporal variations of UV values are investigated.

GRAPHICAL ABSTRACT



ARTICLE INFO

Article history:

Received 22 January 2020

Received in revised form 15 May 2020

Accepted 16 May 2020

Available online 19 May 2020

Editor: Pingqing Fu

Keywords:

Surface solar Ultraviolet radiation

Physically broadband model

FASTUV

China

ABSTRACT

The climatic characteristics of solar Ultraviolet radiation (UV) are of vital importance for the climate change and photochemical reactions. High-quality records of solar UV radiation are the premise for solar UV researches and applications, but solar UV radiation observations are sparse around the world. Among all wavelength of UV radiations, only UVA (0.315–0.400 nm) and UVB (0.280–0.315 nm) could reach the earth surface. This study attempted to develop a novel efficient physically broadband parameterization (hereafter, FASTUV) for estimating surface solar UV radiation (0.280–0.400 μm) in all-sky conditions based on Leckner's spectral model for calculating shortwave solar radiation, using MERRA_2 reanalysis data. The Quadratic polynomial formula and artificial neural networks were used to calculate the cloud transmittance for UV, using sunshine durations measurements at 2474 CMA stations. The surface solar UV radiation measurements at 29 CERN (The Chinese Ecosystem Research Network) stations were used for validating the estimated UV values. The result showed the FASTUV model could be used for estimating UV values with high accuracy, strong robustness and fast speed. Then, the spatial and temporal variation of surface solar UV radiation in China were revealed. The result indicated that the Qinghai Tibetan Plateau and the Palmer Plateau has always been the areas with highest UV values, while the Northeastern China is the area with the lowest UV values. Meanwhile, the FASTUV model have been packaged into a software namely 'FASTUV_V1.0'. We provide the executable file of FASTUV model in publicly available repository: <https://doi.org/10.6084/m9.figshare.11409666>.

© 2020 Elsevier B.V. All rights reserved.

* Corresponding author at: Hunan Key Laboratory of Remote Sensing of Ecological Environment in Dongting Lake Area, School of Geography and Information Engineering, China University of Geosciences, Lumo road 388, Hongshan District, Wuhan 430074, China.

E-mail address: 2015102050003@whu.edu.cn (L. Wang).

1. Introduction

Solar Ultraviolet radiation (UV) is the electromagnetic radiation in spectral range of $0.100\text{ }\mu\text{m}$ to $0.400\text{ }\mu\text{m}$, which is involved in lots of chemical and biological processes and responsible for the ozone variation in the stratosphere (Calkins and Thordardottir, 1980; Williamson et al., 2014). The change of ultraviolet radiation will also directly affect human health (Madronich and de Gruyl, 1993). The wavelength of UV radiation is further subdivided into UVA ($0.315\text{--}0.400\text{ nm}$), UVB ($0.280\text{--}0.315\text{ nm}$), and UVC ($0.100\text{--}0.280\text{ nm}$). Among them, only UV-A and a small amount of UV-B could reach the earth surface (Dayan, 1993).

Accurate observation and determination of surface solar UV radiation ($0.280\text{--}0.400\text{ }\mu\text{m}$) is the premise for investigating the effect of surface UV values on human health and natural environment (Hu et al., 2017; Liu et al., 2017). The UV observation was carried out gradually in the end of 20th century after the discovery of Antarctic ozone hole by Farman et al. (1985). The United States Antarctic Program, National Science Foundation established a high-latitude monitoring UV observation network in 1988 (Booth et al., 1994). The USDA (United States Department of Agriculture) carried out an observation and research program of UV in 1992, to investigate the influence of the UV variation on agricultural production (Bigelow et al., 1998). In China, the Brewer ultraviolet radiation ground-based observation system was established at the Waliguan global atmospheric station and the Zhongshan scientific research station in Antarctica in 1990s, proving long-term continuous UV observation, which marks the beginning of the UV observation network in China (Bo et al., 2009). The CERN network was established in 2004, providing long-term meteorological measurements and solar radiation observations at about 40 ground-based stations covering mainland China, including the high-quality UV measurements (Hu et al., 2007). However, these UV observation stations are still too sparse for UV research and related applications.

Numerous models have been proposed for estimating UV values (Arola, 2002). The empirical models assumed that there is a certain mathematical relationship between solar UV radiation and climate change factors (air quality, ozone concentration and water vapor content etc.) (Nunez et al., 1994; Peng et al., 2015; Wang et al., 2015; Hu et al., 2017; Habte et al., 2019). Feister and Grasnick (1992) found that the ratio between solar UV radiation and global solar radiation (hereafter, UV/G) is 0.026 at Postdam in Germany. Madronich et al. (1998) revealed that the UV/G is 0.029 in Valencia (Spain). Foyo-Moreno et al. (1999) proposed that UV/G is about 0.04 at Granda (Spain). Cañada (2003) pointed out that the UV/G were 0.05 (0.044–0.056) at Valencia and 0.042 (0.039–0.045) at Córdoba in Spain, respectively. Hu et al. (2010) revealed that the UV/G are closely correlated with aerosol optical depth and water vapor content, the UV/G for arid area and semi-arid area were 0.035 ± 0.003 and 0.041 ± 0.006 , respectively. However, it could be seen from above changing UV/G values that the empirical models for estimating UV values are not reliable with poor universality. The physically based models could effectively estimate surface UV values, owing to considering the radiation dumping processes in the atmosphere. Leckner (1978) developed a spectral model for calculating surface solar radiation between 0.280 and $4.000\text{ }\mu\text{m}$, taking into account of the Rayleigh scattering, the uniformly mixed gas absorption, the aerosol extinction, the ozone absorption, and the water vapor absorption. Gueymard (1995) proposed a simple model of the atmospheric radiative transfer (SMASTS2) model for predicting shortwave solar radiation ($0.280\text{--}4.000\text{ }\mu\text{m}$). Lean et al. (1997) developed a physically based parametrization for calculating UV values ($0.200\text{--}0.400\text{ }\mu\text{m}$). Katsambas et al. (1997) proposed a theoretical approach of the surface UV values for Athens in Greece. Other models like REST2 (Gueymard, 2008), Bird's model (Bird, 1984) and Iqbal's model (Iqbal, 2012) could also be used for estimating surface solar UV radiation. However, these models are limited by the rough spatial and temporal resolution of the ground based meteorological stations.

Satellite signals, such as the Total Ozone Mapping Spectrometer (TOMS), the Global Ozone Monitoring Experiment 2 (GOME-2), the ozone measuring instrument (OMI), the scanning imaging absorption spectrometer for atmospheric cartography (SCIAMACHY), and the Meteorological Operational satellite program (MetOp), could provide land and atmosphere information with high spatial and temporal resolutions for estimating surface solar UV radiation (Krotkov et al., 1998; Krotkov et al., 2001; Tanskanen et al., 2006; Wang et al., 2017; Singh et al., 2018; Qin et al., 2018a; Kanellis, 2019). Verdebout (2000) presented a method for generating UV values throughout Europe based on Look-up Table method with spatial resolution of 0.05° , using GOME, Meteosat and ancillary geophysical data. The estimated UV values showed good agreement with UV measurements at Ispra. Láska et al. (2011) proposed a non-linear regression model with a hyperbolic transmissivity function for predicting UV values using satellite ozone records derived from EOS-Aura spacecraft. The model could effectively estimate UV values with 98.6% variability of the EUV radiation. Lamy et al. (2018) developed local parameterization for retrieval UV values using satellite records derived from SBUV2, OMI-DOAS and MLS satellite. However, satellite signals are susceptible to cloud and bad weather. Therefore, the accuracy and spatial-temporal continuity of satellite signals could not meet the requirement for UV researches in larger spatial-temporal scales. Cadet et al. (2017) evaluated the accuracy of the UV records derived from OMI/AURA experiment at 6 African stations. The result indicated that the relative UV difference between ground UV measurements and UV records from OMI/AURA UV is in range of 0%–45% depending on the location and seasons. As an alternative, reanalysis data including ERA5 (Babar et al., 2019; Wei et al., 2019b), NCEP-DOE AMIP-II reanalysis (Kanamitsu et al., 2002), the CRU JRA V2.0 (Beck et al., 2017), CFSR (The Climate Forecast System Reanalysis) (Fukui et al., 2014), and MERRA_2 (Hodges et al., 2011; Qin et al., 2018b) are available sources providing land and atmosphere products with acceptable accuracy and high spatiotemporal continuity covering the mainland of China.

This study attempted to develop a physically based broadband model for estimating surface solar UV radiation with fast speed, acceptable accuracy and excellent spatial-temporal continuity. Firstly, an efficient physically based broadband model (hereafter, FASTUV) for estimating surface solar UV radiation ($0.280\text{--}0.400\text{ }\mu\text{m}$) in clear sky condition was developed using MERRA_2 reanalysis products. Meanwhile, we developed an AI model for correcting the cloud effect on UV values in all sky conditions. Then, the model accuracy was evaluated using surface solar UV radiation measurements at 29 CERN stations. Finally, the spatial-temporal characteristics of surface solar UV radiation over mainland China were revealed. The model would assist in solar resource and ecological system studies.

2. Input and validation data

2.1. Ground daily UV observations

Daily surface solar UV radiation (UV) measurements during 2005–2015 at 29 CERN stations over mainland China were used for model construction and validations of FASTUV model. These measurements have been checked for ensuring data quality using various data quality control methods. Fig. 1 showed the spatial distribution of the 29 selected CERN stations. These stations covered most areas of China ($18.21^\circ\text{N}\text{--}47.58^\circ\text{N}$, $87.93^\circ\text{E}\text{--}133.51^\circ\text{E}$) with distinct climatic and terrain features. Meanwhile, sunshine duration measurements at 2474 CMA stations were used to calculate the cloud transmittance for UV.

2.2. MERRA_2 reanalysis products

The MERRA_2 products provided by the Global Modeling and Assimilation Office (GMAO) in NASA were used as input parameters in FASTUV

model. The MERRA_2 dataset shows good spatial and temporal continuity with long temporal range (1980–present) throughout China. Detailed information about the MERRA_2 dataset that were used in this study are shown in Table 1.

2.3. Sunshine duration measurements

The cloud effects on surface solar UV radiation could be calculated using sunshine duration observations at 2474 CMA stations over mainland China. However, the point density of these CMA stations was still too low for predicting surface solar UV radiation throughout China (Qin et al., 2019). Thus, a grid sunshine duration dataset covering the mainland of China were generated using Anusplin package. The Anusplin package contains FORTRAN programs for fitting surfaces to noisy data as functions of one or more independent variables, through comprehensive statistical analyses, data diagnostics and spatially distributed standard errors. Detail description of the Anusplin tool could be found in Ref (Hutchinson and Xu, 2004).

3. Method

3.1. Calculating UV values in clear skies

When solar rays passing through the top of the atmosphere, solar radiation would undergo five main radiation damping processes. Solar radiation would firstly be absorbed by ozone which mainly occurred in the ozonosphere. Further radiation damping processes including water vapor absorption, aerosol extinction, cloud extinction, cloud scattering and other atmospheric gasses were mainly occurred in the troposphere, which vary with time and space in different climate zones and terrains. The main idea of the FASTUV model is to develop a broadband parameterization for calculating UV values under clear skies, and then to quantify the cloud effects in all-sky conditions using sunshine-duration measurements. The clear-sky spectral transmittance model proposed by Leckner

Table 1
Basic information about the MERRA_2 products used in this study.

Product name	Parameters name	Short name
Inst3_2d_gas_Nx	Aerosol optical depth (550 nm)	AODANA
inst1_2d_asn_Nx	Surface pressure	PS
inst1_2d_asn_Nx	Total column ozone	TO3

(1978) is the basis for FASTUV model. The Leckner's model could be briefly expressed as follows:

$$UV_{clr} = \frac{1}{\Delta t} \left\{ \int_{\Delta t} \left(g_{b,i}^{clr} + g_{d,i}^{clr} \right) dt \right\} \quad (1)$$

$$g_{b,i}^{clr} = TOA(d_0/d)^2 (\sinh) \bar{\tau}_b \quad (2)$$

$$g_{d,i}^{clr} = TOA(d_0/d)^2 (\sinh) \bar{\tau}_d \quad (3)$$

$$\bar{\tau}_b = TOA^{-1} \int_{0.28}^{0.40} Q_{00}(\lambda) \tau_g^\lambda \tau_R^\lambda \tau_w^\lambda \tau_o^\lambda \tau_a^\lambda d\lambda \quad (4)$$

$$\bar{\tau}_d = TOA^{-1} \int_{0.28}^{0.40} Q_{00}(\lambda) \tau_g^\lambda \tau_w^\lambda \tau_o^\lambda (1 - \tau_R^\lambda \tau_a^\lambda) d\lambda \quad (5)$$

$$TOA = \int_{0.28}^{0.40} Q_{00}(\lambda) d\lambda \quad (6)$$

where UV_{clr} is the surface solar UV radiation in clear sky condition; Δt is the integration period; $g_{b,i}^{clr}$ and $g_{d,i}^{clr}$ are the instantaneous beam and diffuse irradiance for UV band in clear sky condition, respectively; λ (nm) is the wavelength; d_0/d is the eccentricity correction factor for the mean sun-Earth distance; h is the solar elevation angle; $\bar{\tau}_b$ and $\bar{\tau}_d$ are the transmittance for beam and diffuse surface solar UV radiation, respectively; TOA is the spectral irradiance at the mean distance between the sun and Earth; τ_g , τ_R , τ_w , τ_o , and τ_a

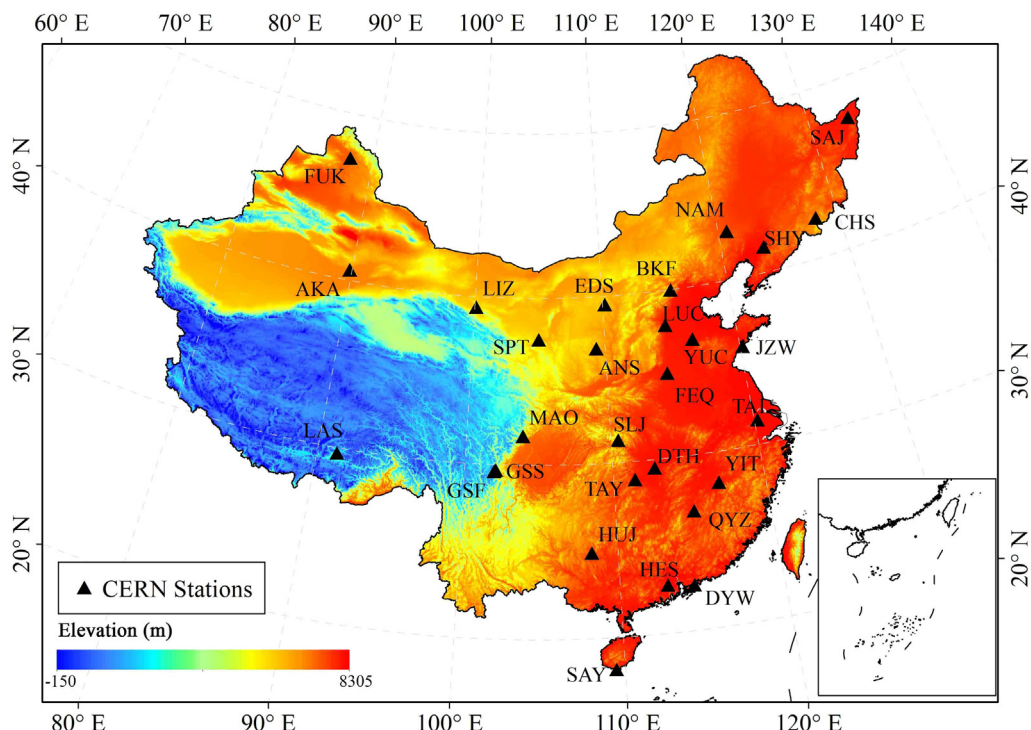


Fig. 1. The spatial distribution of the 29 CERN stations that were used in this study.

are the spectral transmittances for uniformly mixed gas absorption, Rayleigh scattering, water vapor absorption, ozone absorption, and aerosol extinction, respectively. τ_g , τ_R , τ_w , τ_o , and τ_a could be calculated using following equations:

$$\tau_g^\lambda = \exp\left\{ \left[-1.41k_g^\lambda m' \right] / \left[1 + 118.3k_g^\lambda m' \right]^{0.45} \right\} \quad (7)$$

$$\tau_R^\lambda = \exp(-0.008735m'\lambda^{-4.08}) \quad (8)$$

$$\tau_w^\lambda = \exp\left\{ \left[-0.2385k_w^\lambda mw \right] / \left[1 + 20.07mw \right]^{0.45} \right\} \quad (9)$$

$$\tau_o^\lambda = \exp(-mlk_o^\lambda) \quad (10)$$

$$\tau_a^\lambda = \exp(-m\beta\lambda^{-1.3}) \quad (11)$$

where k_g , k_w , and k_o represent the absorption coefficients for uniformly mixed gas absorption, water vapor absorption, and ozone absorption, respectively; w is the precipitable water vapor; l is the ozone layer thickness; β is the Angstrom turbidity coefficient; m is the relative air mass; m' is the pressure-corrected relative air mass; h is the solar elevation angle; ps is the surface pressure; p_0 is the standard atmospheric pressure.

The solar extraterrestrial radiation in different spectral band and the spectral transmittances for each radiation dumping processes are irregular. In Leckner's spectral model, the integral values in Eqs. (4)–(6) are obtained using numerical integration. However, the numerical integration method is time consuming which would limit the practical applications of Leckner's spectral model. Therefore, simplified parametrizations are used to calculate $\bar{\tau}_b$ and $\bar{\tau}_d$, which are described as follows:

$$\bar{\tau}_b \approx \tau_R \tau_o \tau_a \quad (12)$$

$$\bar{\tau}_d \approx 0.5 \tau_o (1 - \tau_R \tau_a) \quad (13)$$

where, τ_R , τ_o and τ_a represent the broadband transmittance for Rayleigh scattering, ozone absorption, and aerosol extinction in UV band, respectively. The transmittances in UV band for water absorption and uniformly mixed gas absorption are relatively high, thus they were not considered in Eqs. (10) and (11). τ_R , τ_o and τ_a could be defined as follows:

$$\bar{\tau}_j \approx \text{TOA}^{-1} \int_{0.28}^{0.40} Q_{00}(\lambda) \tau_j^\lambda d\lambda \quad (14)$$

where j can be R, o, or a, representing the transmittance for Rayleigh scattering, ozone absorption, and aerosol extinction, respectively. As shown in Eqs. (7)–(11), $\bar{\tau}_j$ is a function of l , β , m and m' . Therefore, $\bar{\tau}_j$ could be approximated using following quadratic exponential formula and power function:

$$\bar{\tau}_j \approx \exp(a_j X^{b_j}) + \exp(c_j X^{d_j}) \quad (15)$$

$$\bar{\tau}_j \approx a_j X^{b_j} + c_j \quad (16)$$

where X could be m' , $m\beta$, and ml . a_j , b_j , c_j and d_j are the regression coefficients for different values of X .

In this study, 2,490,410 data samples covered 29 selected CERN stations are used to fit a_j , b_j , c_j and d_j in Eq. (15). Fig. 2 is the scatter plot showing the relationship between $\bar{\tau}_j$ and atmospheric parameters (l , β , m and m'). The fitting line perfectly fitted the scatter points in Fig. 2. The R of the fitting line for Rayleigh scattering, ozone absorption and aerosol extinction are 0.9999, 0.9998 and 0.9999, respectively. Therefore, $\bar{\tau}_j$ could be effectively parameterized using quadratic

exponential formula and power function in Eqs. (15) and (16). The fitted formulas are given as:

$$\tau_R = \exp(-1.0629m^{0.3484}) + \exp(-0.4904m^{0.6513}) \quad (17)$$

$$\tau_o = -0.8313ml^{0.0586} + 1.624 \quad (18)$$

$$\tau_a = \exp(-4.5664m\beta^{0.3943}) + \exp(-3.5678m\beta^{0.6053}) \quad (19)$$

As well known, the broadband model is more unstable and inaccurate than spectral models, due to ignoring the spectral transmittances for Rayleigh scattering, ozone absorption, aerosol absorption and aerosol extinctions. However, as shown in Fig. 3, the estimated UV values by FASTUV model showed high agreements with the estimated UV values by Leckner's spectral model with RMSE, MAE and R of 0.0019 Wm⁻², 0.0013 Wm⁻² and 0.9999, respectively. Therefore, the FASTUV model could save complex and time-consuming integral calculations of narrow-band transmittances for Rayleigh scattering, ozone absorption, and aerosol extinction, while ensuring the accuracy for estimating surface solar UV radiation.

Fig. 4 illustrated the flowchart of FASTUV models. Firstly, the clear sky transmittances for Rayleigh scattering, ozone absorption, aerosol extinction for solar UV radiation were calculated using Eqs. (17), (18) and (19). Then, $\bar{\tau}_b$ and $\bar{\tau}_d$ are calculated using Eqs. (12) and (13). Then, the g_b^{clr} , g_d^{clr} and UV_{clr} are calculated using Eqs. (1), (2) and (3). Meanwhile, the cloud transmittances for solar UV radiation are calculated based on artificial intelligence method (ANN) and Quadratic polynomial formula (QPF) using sunshine duration, date (year, month and day), locations (latitude and longitude), and UV_{clr} . Finally, the surface solar UV radiation in all sky condition are calculated.

3.2. Cloud effects on surface solar UV radiation

It is certain that solar UV radiation would be reflected and scattered in the cloud layer (McKenzie et al., 1998; Sabburg and Wong, 2000; Foyo-Moreno et al., 2003). However, the cloud was considered to be the most uncertain factor for predicting surface solar irradiance, owing to the variation of the cloud shape, cloud type and cloud phase in various climatic zones and terrain features (Tang et al., 2018). Thus, quantifying the cloud effect on solar rays is of vital importance for improving the accuracy in estimating the surface solar UV radiation.

3.2.1. Quadratic polynomial formula

The cloud transmittance for solar radiation was defined by Angstrom and further improved by Prescott as the ratio of solar radiation in all sky to the solar radiation in clear sky condition. Following the idea of the Ångström-Prescott equation (Prescott, 1940), Yang et al. (2010) parameterized the cloud transmittance on solar radiation as a function of the relative sunshine duration (n/N). On the basis of the parameterization by Yang, we defined the cloud transmittance for surface solar UV radiation (τ_c) as a quadratic polynomial formulation:

$$\tau_c = \frac{UV_{all}}{UV_{clr}} = a + b \left(\frac{n}{N} \right) + c \left(\frac{n}{N} \right)^2 \quad (20)$$

The UV_{all} and UV_{clr} are the surface solar UV radiation in all-sky and clear-sky conditions, respectively; n and N are the sunshine duration and the maximum possible sunshine duration, respectively; a , b and c are the regression coefficient.

Fig. 5 showed the relationship between the cloud transmittance for daily UV values and the relative sunshine duration. The calibrated

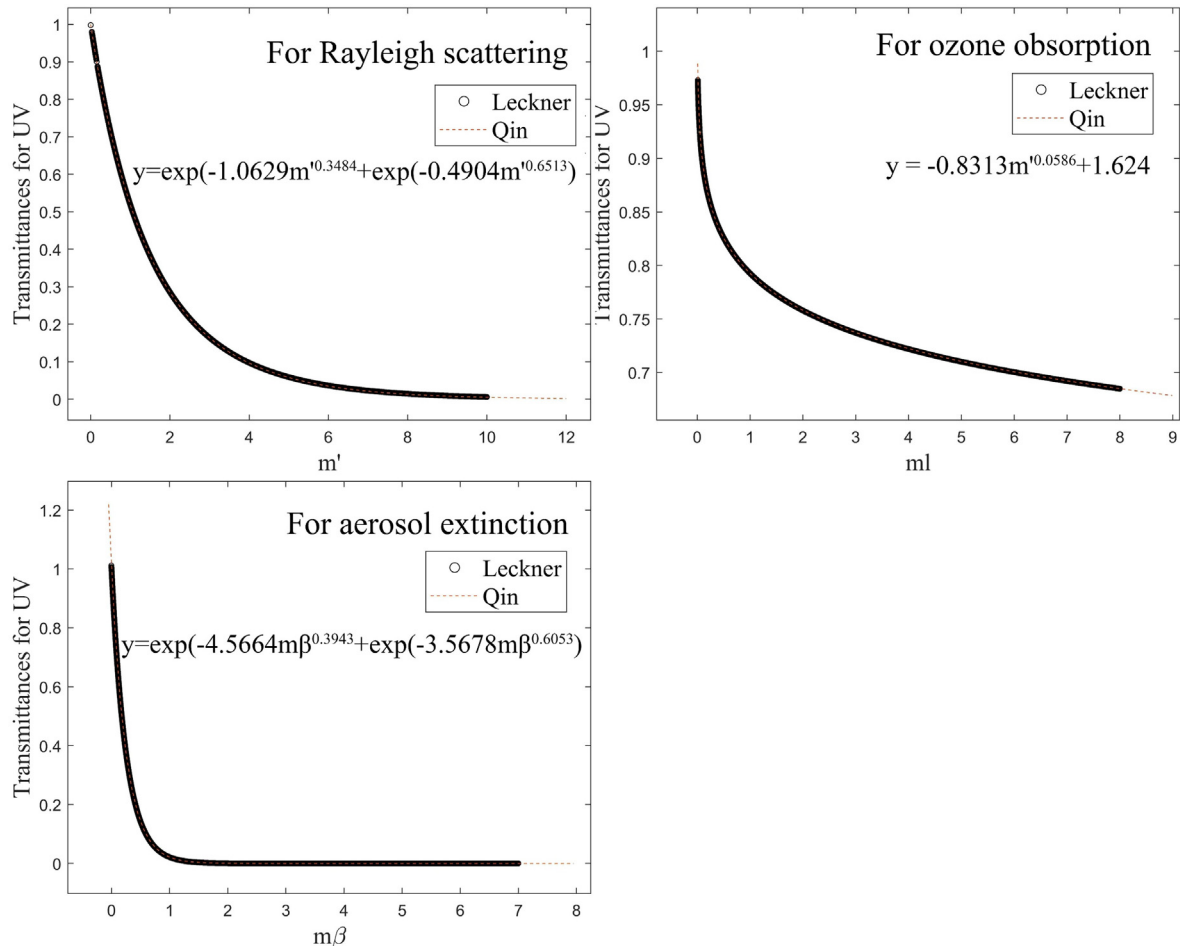


Fig. 2. Comparison of UV broadband transmittances for individual extinction processes between spectral integration and parameterization for Rayleigh scattering [Eq. (17)], aerosol scattering [Eq. (18)], and ozone absorption [Eq. (19)].

cloud transmittances for daily UV values are shown as following equations:

$$\tau_c = 0.267 + 1.099 \frac{n}{N} - 0.567 \frac{n^2}{N} \quad (21)$$

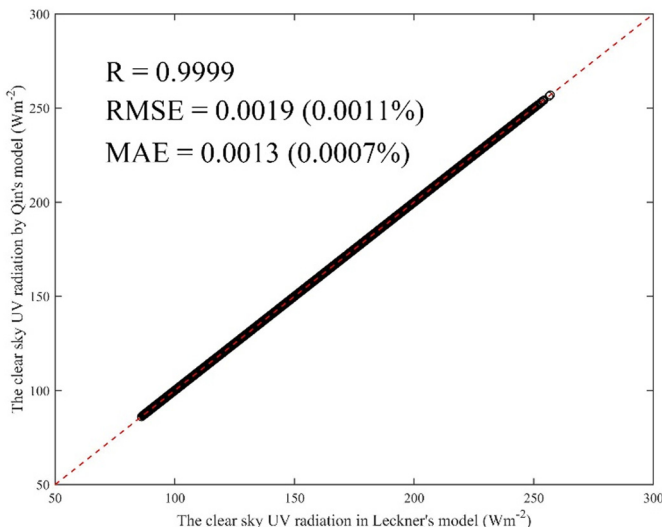


Fig. 3. Comparison between the estimated UV values by FASTUV model and Leckner's spectral model without considering the cloud transmittance.

The quadratic polynomial formula has always been used to estimate the cloud transmittance for solar radiation rapidly in previous studies. However, as shown in Fig. 5, the scatter points are in decentralized distribution. Meanwhile, the cloud transmittances were greater than 1.0, when UV_{all} were greater than UV_{clr} values. Moreover, the regression coefficients vary greatly using data samples at different CERN stations. Thus, there are large uncertainties in calculating τ_c using QPF method, which would deduce the accuracy of the estimated UV values.

3.2.2. Artificial neural network

In this study, the artificial neural network (ANN) is applied to directly construct a nonlinear relationship between the UV_{all} , UV_{clr} and geographical elements (sunshine duration, geographical location and season). The ANN model was constructed by three layers including input layer (UV_{clr} , sunshine duration, maximum sunshine duration, latitude (lat), longitude (lon), year, month, the day in the year (Dayth)), hidden layer and output layer (UV_{all}). The hidden layer is formed by 10 neurons. In this study, 70% of the dataset were randomly chosen for training stages, and the remaining 30% for testing stages. Fig. 6 showed the flowchart of the ANN model.

3.3. Comparisons of measures of fit

The measures of fit-used in the present study include the root mean square error (RMSE, Wm^{-2}), the mean absolute bias error (MAE, Wm^{-2}), the relatively root mean square error (RMSD, %), the relatively

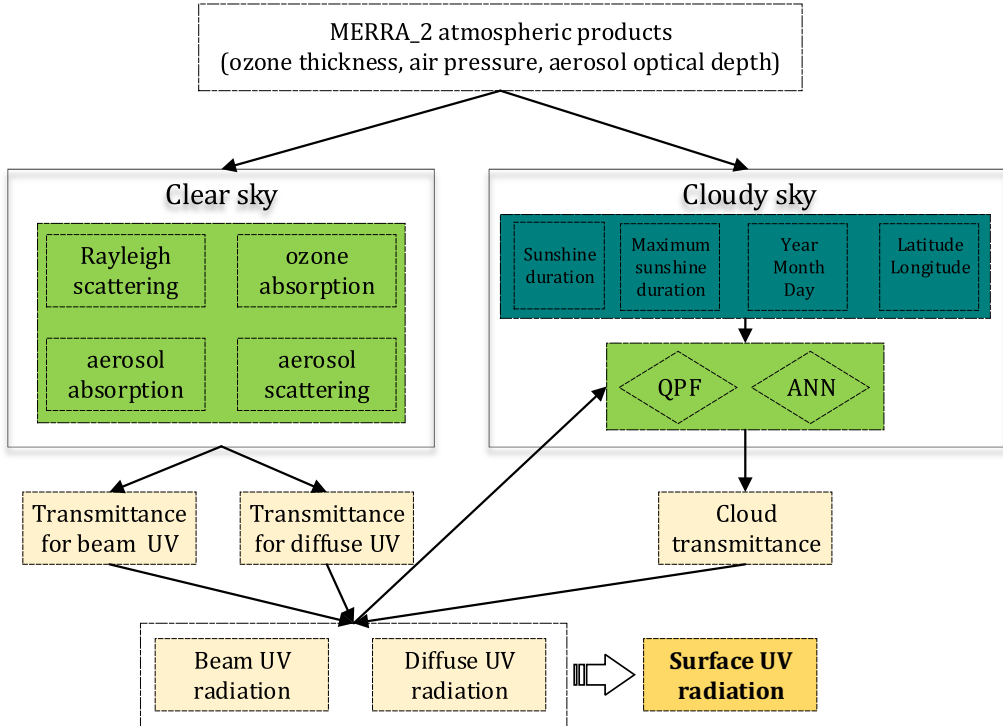


Fig. 4. Flowchart of the proposed model for estimating surface solar UV radiation.

mean absolute bias error (MAD, %), the correlation coefficient R, which could be expressed as:

$$RMSE = \sqrt{\frac{1}{N} \sum_{i=1}^n (e_i - o_i)^2} \quad (22)$$

$$MAE = \frac{1}{N} \sum_{i=1}^n |e_i - o_i| \quad (23)$$

$$RMSD = \frac{100}{\bar{o}_i} \times \sqrt{\frac{1}{N} \sum_{i=1}^n (e_i - o_i)^2} \quad (24)$$

$$MAD = \frac{100}{\bar{o}_i} \times \frac{1}{N} \sum_{i=1}^n |e_i - o_i| \quad (25)$$

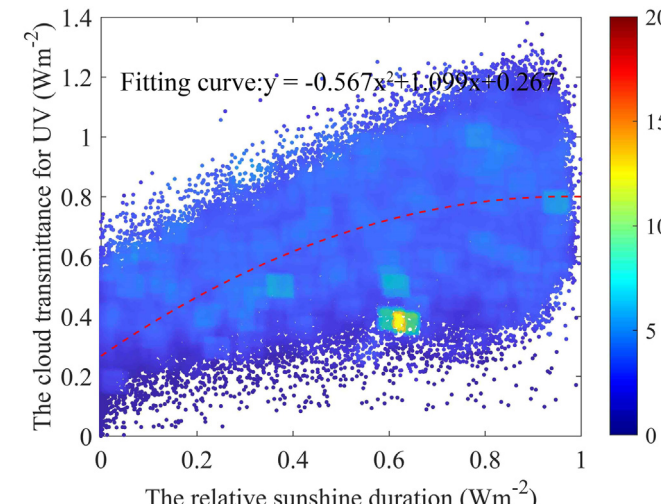


Fig. 5. The relationship between the relative sunshine duration and the cloud transmittances.

$$R = \frac{\sum_{i=1}^n (e_i - \bar{e})(o_i - \bar{o})}{\sqrt{\sum_{i=1}^n (e_i - \bar{e})^2} \sqrt{\sum_{i=1}^n (o_i - \bar{o})^2}} \quad (26)$$

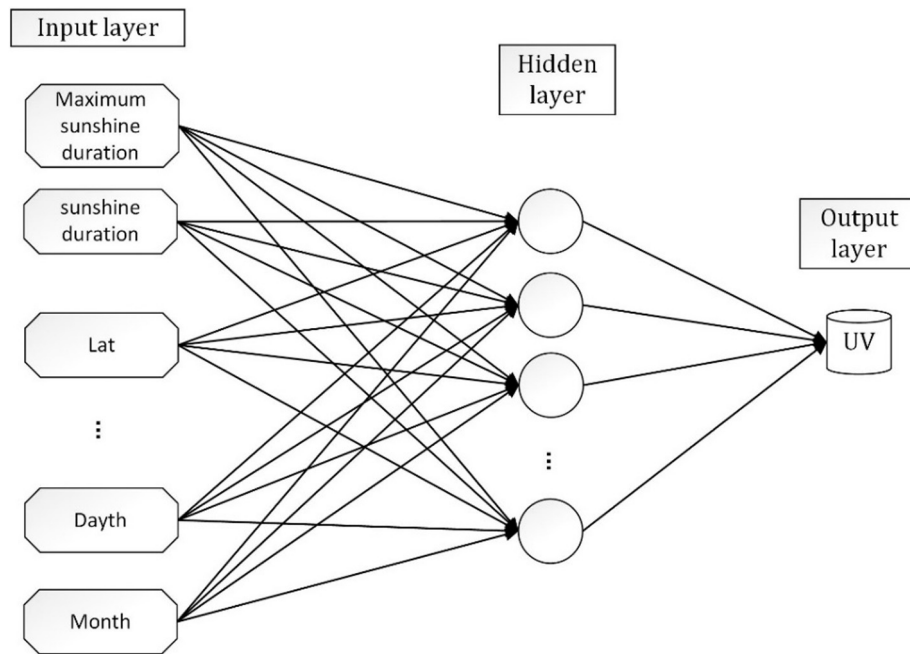
where, N and bar respectively indicated the number of data and mean of the variables; e_i and o_i were the modeled and observed UV values.

4. Result and analysis

4.1. Validation of UV estimations with ground UV measurements

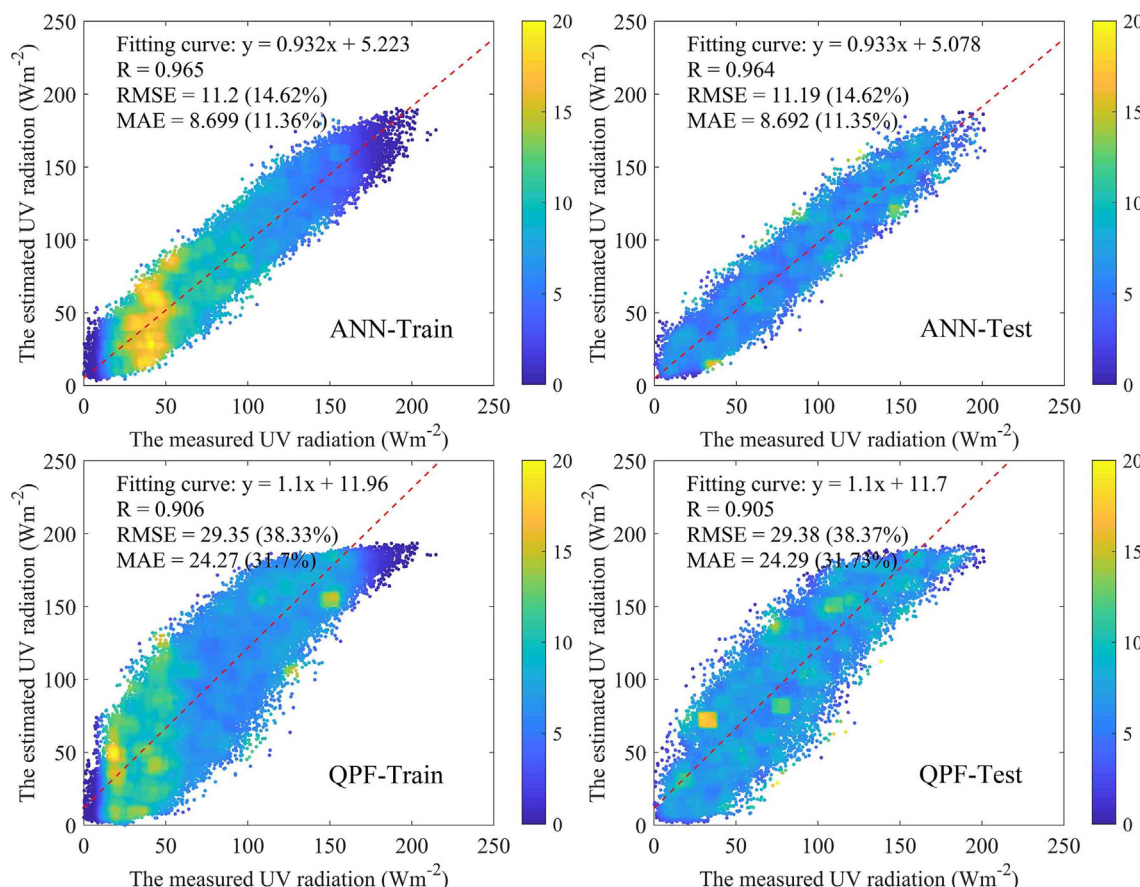
Daily UV measurements (104,278 samples) during 2005–2015 at 29 CERN stations were used for evaluating the model accuracy of the daily estimated UV values by FASTUV model. Fig. 7 was the scatter plot showing the model accuracy of FASTUV model using different cloud transmittance calculating method. It was clear that the estimated result using ANN method showed better agreements with UV observations than that for QPF method, because the ANN method could effectively reflect the nonlinear relationship between the cloud transmittance and geographical elements. In training stages, the RMSE, MAE, RMSD, MAD, and R for the estimated result using QPF method are 29.350 Wm^{-2} , 24.270 Wm^{-2} , 38.33%, 31.70% and 0.906, respectively; the RMSE, MAE, RMSD, MAD, and R for the estimated result using ANN method were 11.200 Wm^{-2} , 8.699 Wm^{-2} , 14.62%, 11.36% and 0.965, respectively. In testing stages, the RMSE, MAE, RMSD, MAD, and R for the estimated result using method QPF are 29.380 Wm^{-2} , 24.290 Wm^{-2} , 38.37%, 31.73% and 0.905, respectively; the RMSE, MAE, RMSD, MAD, and R for the estimated result using ANN method were 11.190 Wm^{-2} , 8.692 Wm^{-2} , 14.62%, 11.35% and 0.964, respectively.

Figs. 8 and 9 indicated the validation results of the estimated surface solar UV radiation values by FASTUV model at 29 CERN stations using QPF and ANN method, respectively. Tables S1 and S2 illustrated the statistical indicators representing the model accuracy of the estimated UV values in training and testing stages using different cloud transmittance methods. The results indicated that the estimated UV values using ANN method preformed superior than that using QPF at all 29 selected CERN stations, because ANN method could better reflect the inner nonlinear

**Fig. 6.** The flowchart of the ANN model.

relationship between the sunshine duration and cloud transmittance. The estimated UV values using ANN method was closely correlated with UV measurements with low RMSE (9.092 Wm^{-2} – 15.190 Wm^{-2}), low MAE (6.909 Wm^{-2} – 12.217 Wm^{-2}), low RMSER

(8.004% – 25.769%), low MAER (6.263% – 20.726%) and high R (0.934 – 0.980). In contrast, the estimated UV values using QPF method could barely match the measured UV values with higher RMSE (11.240 Wm^{-2} – 70.234 Wm^{-2}), higher MAE (13.456 Wm^{-2} –

**Fig. 7.** Validation of the estimated surface solar UV radiation using different cloud transmittance calculating method in China. (QPF and ANN represent the quadratic polynomial formula and the ANN model, respectively; 'Train' and 'Test' denote the training state and testing state, respectively.).

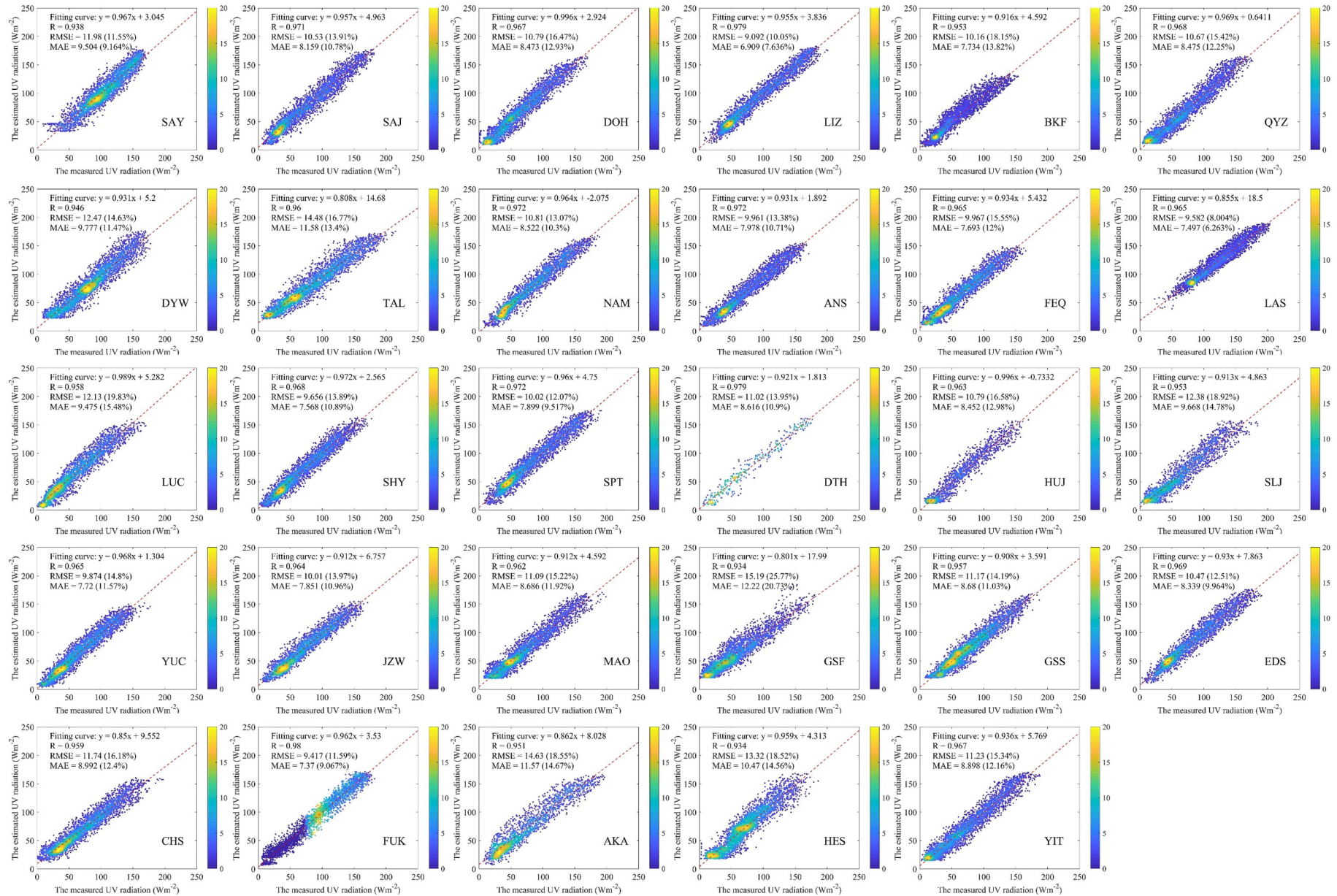


Fig. 8. Validation of the estimated surface solar UV radiation using ANN method in different stations in China.

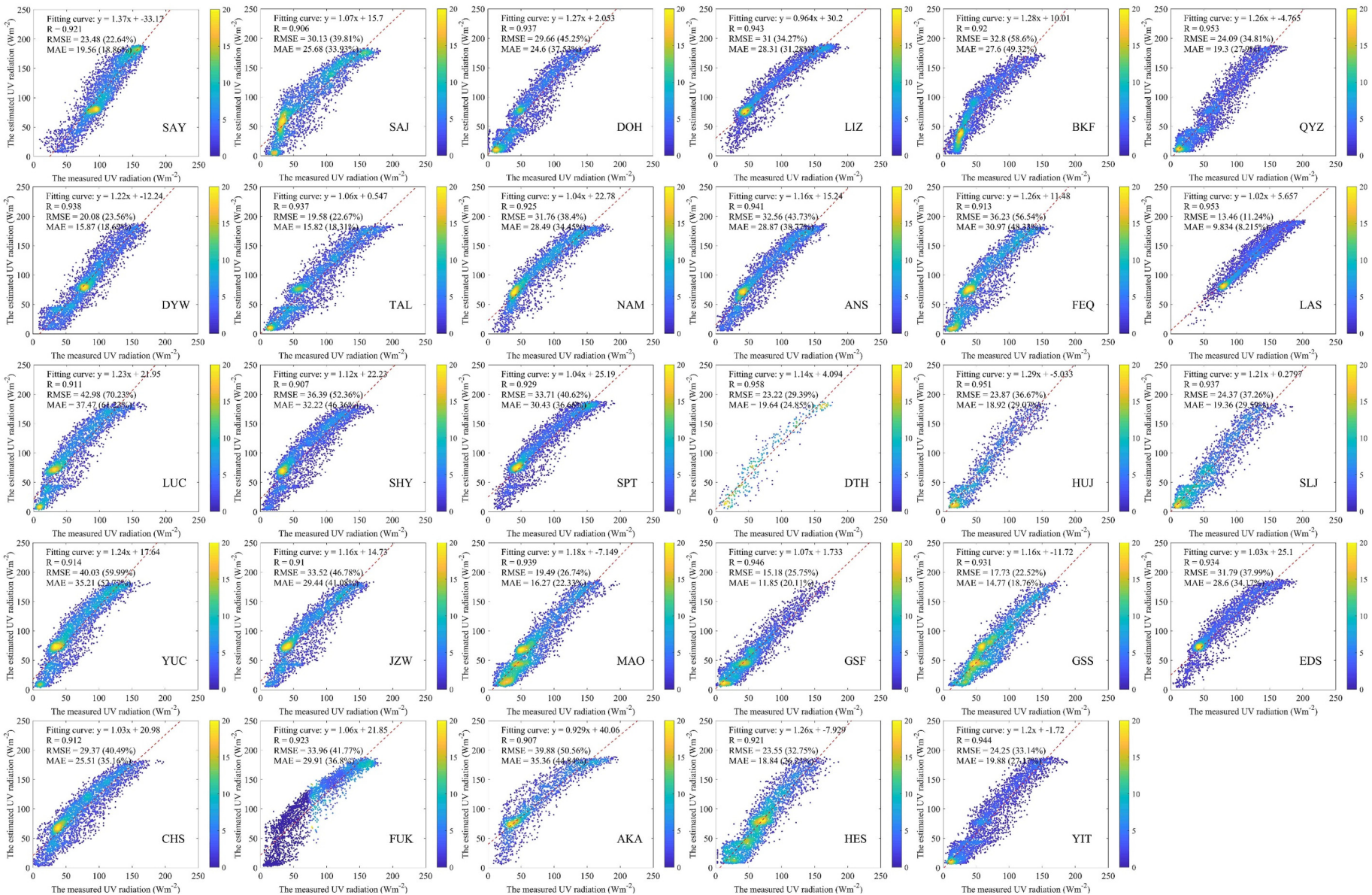


Fig. 9. Validation of the estimated surface solar UV radiation using ANN method in different stations in China.

42.975 Wm^{-2}), high RMSER (8.215%–61.230%), higher MAER (9.834%–37.466%), and lower R (0.906–0.958).

In all, the new proposed FASTUV model has been proved to be an efficient model for estimating surface solar UV radiation with high accuracy and good robustness.

4.2. The spatial and temporal variation of UV radiations in China

By applying the FASTUV model, a grid UV dataset (0.50° (lat) * 0.625° (lon)) in 2014 throughout China were constructed. Then, the spatial and temporal variations of surface UV values over mainland China in 2014 were investigated. Fig. 10 showed the spatial variation of the annual mean UV values in 2014 in China. Generally, the UV values was gradually decreased from Western China to Southeastern China, owing to the gradually stronger radiation dumping processes from Western China to Eastern China. From Northern China to Southern China, the UV values has a trend of first rising and then declining, owing to the high latitude in Northern China and the strong radiation dumping processes in Southern China. The Qinghai Tibetan Plateau and the Pamirs was the area with the highest UV values across China, because the atmospheric extinction effects on UV radiations are weak in Plateau areas. The most areas of Xinjiang and Inner Mongolia were also areas with high UV values, owing to the dry air conditions there. In contrast, the Northeastern China was the area with the lowest UV values, because the extraterrestrial radiation reaching the top of the atmosphere is lower than that in other areas in China. The Sichuan Basin was also an area with low UV values, due to the perennial cloudy weather and strong atmospheric extinction effect there.

Fig. 11 illustrated the month variation of daily mean UV value in 2014 in China. The result showed that the UV value gradually increased from January to July, then gradually decreased from August to December, because of the monthly variations of the annual cycle of solar zenith and the maximum sunshine duration in China. The Plateau areas in Western China were always the area with high UV values. The Tarim Basin, Jungar Basin, and Inner Mongolia are also an area with high UV values, but the UV values there showed distinct seasonal variety because of the seasonal changes of the incoming solar radiations in the atmosphere.

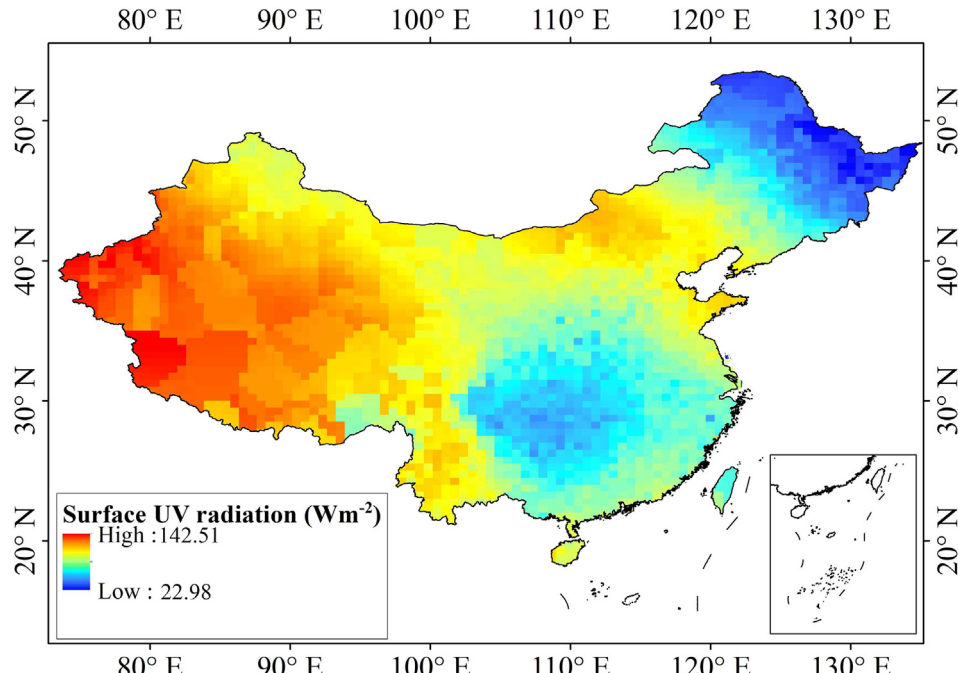


Fig. 10. The spatial distributions of the annual mean UV radiation in 2014 throughout China.

5. Discussion

5.1. Sensitivity analysis for input parameters

In this study, the factorial approach method (Henderson-Sellers, 1993) was introduced to reveal the influence of parameters' fluctuations on modeling UV values. As described in FASTUV model, five input parameters including ps , AOD , loz , sz and TOA are required to run FASTUV model. Among them, sz and TOA are always fixed in certain time and locations. Thus, only AOD , ps and loz were selected to conduct the sensitivity analysis for FASTUV model, because they are more unstable and variable than other input parameters. Limited by computing efficiency, only 1000 samples were randomly selected to conduct this experiment. Six perturbations are assigned to each parameter for FASTUV model (+10%, +20%, +30%, -10%, -20% and -30%), to investigate the partial effects by different parameters, which need 6×3 runs. The RMSE (Wm^{-2}) between the estimated SSR without perturbations and the estimated UV with perturbations was calculated to show the partial effect by each parameter.

Table 2 illustrated the sensitivity analysis result for ps , AOD and loz . It was clear that the partial effects of AOD 's fluctuations on modeling UV values were obviously higher than that for ps and loz , because the aerosol particles have strong absorption and scattering effects on solar radiation (Qin et al., 2018c; Wei et al., 2019a). When AOD values were multiplied by 0.9, 1.1, 0.8, 1.2, 0.7 and 0.9, the RMSE were 2.510, 2.577, 4.756, 5.465, 6.833 and 8.622 Wm^{-2} , respectively. The effects of the perturbations of ps on modeling UV values was also obvious, because the higher the ps is, the stronger the radiation dumping effects is, and vice versa. When ps were multiplied by 0.9, 1.1, 0.8, 1.2, 0.7 and 0.9, the RMSE were 2.102, 2.304, 4.099, 4.738, 5.977 and 7.353 Wm^{-2} , respectively.

5.2. Model computing efficiency

To evaluating the computing speed and model accuracy of FASTUV model, the FASTUV model was compared against the Leckner's spectral model using MATLAB 2015a software on a personal computer with 3.6GHZ Inter i7 CPU and a 64 Gb double data rate type three random-access memory. The data samples that were used to evaluate the

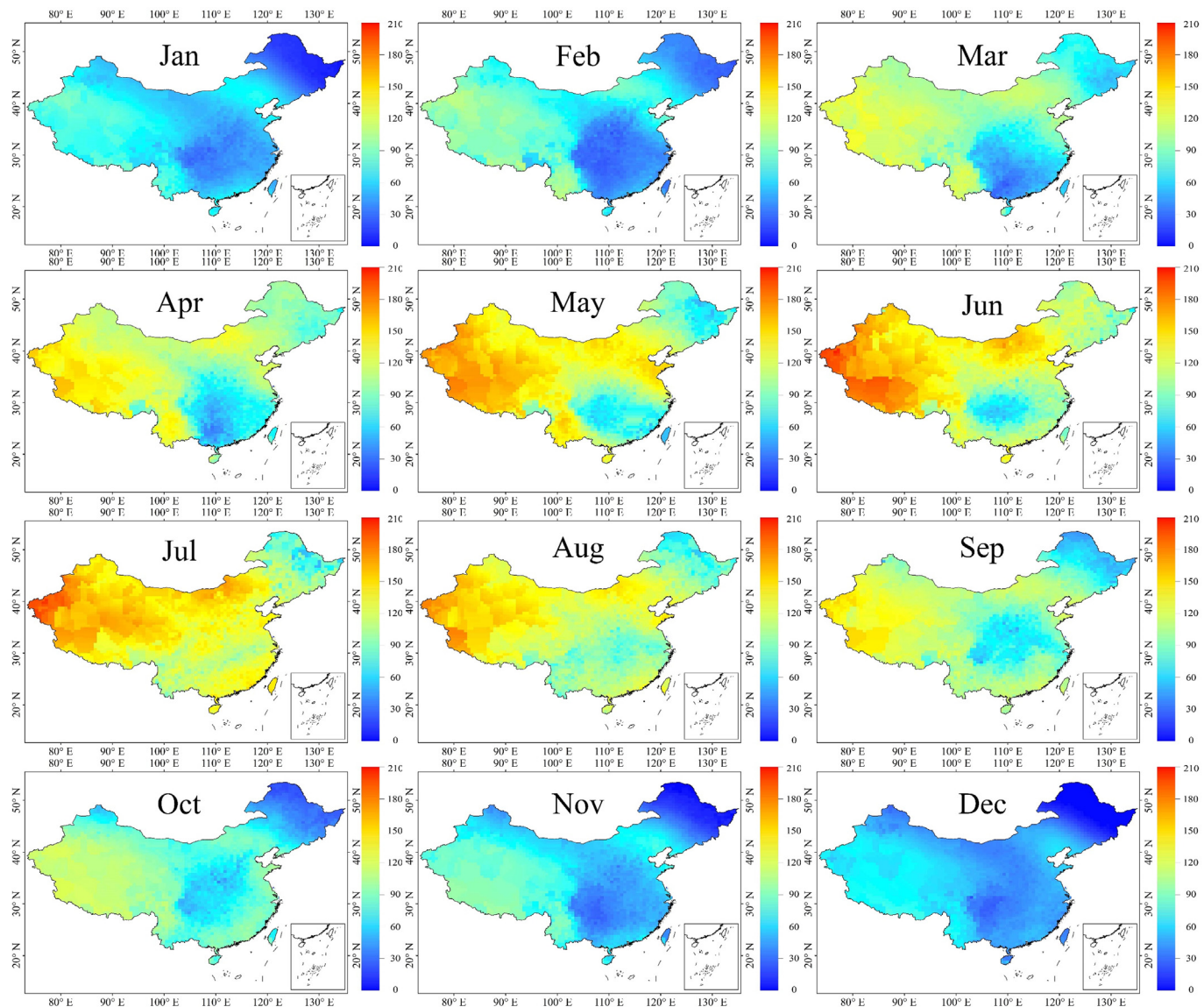


Fig. 11. The spatial distributions of the monthly mean UV radiation in 2014 throughout China.

Table 2
The sensitivity analysis for FASTUV model.

Ps	AOD	loz	RMSE (Wm^{-2})	MEAN (Wm^{-2})
10%	–	–	2.102	4.429
–10%	–	–	2.304	
20%	–	–	4.099	
–20%	–	–	4.738	
30%	–	–	5.977	
–30%	–	–	7.353	
–	10%	–	2.510	5.127
–	–10%	–	2.577	
–	20%	–	4.756	
–	–20%	–	5.465	
–	30%	–	6.833	
–	–30%	–	8.622	
–	–	10%	0.882	2.006
–	–	–10%	1.095	
–	–	20%	1.744	
–	–	–20%	2.241	
–	–	30%	2.541	
–	–	–30%	3.532	

model accuracy in Section 4.1 were reused in this experiment. The result showed that the FASTUV model only takes 31.577 s, but the Leckner's model does about 103.829 s. It could be concluded that the FASTUV model greatly improved the computing efficiency for estimating surface solar UV radiation with comparable accuracy.

5.3. A packaging software for calculating surface solar UV radiation

To facilitate the users of FASTUV model, the newly proposed FASTUV model was made into a packaging software namely 'FASTUV_V1.0' using MATLAB 2015a. The 'FASTUV_V1.0' is provided in publicly available repository: <https://doi.org/10.6084/m9.figshare.11409666>.

The detailed step to run FASTUV_V1.0 are, 1) preparing surface pressure, aerosol optical depth (550 nm), total column ozone and sunshine duration data derived from MERRA_2 products in TXT format ('inputdata.txt' and 'sunshine_duration.txt'); 2) placing 'inputdata.txt' and 'sunshine_duration.txt' in a folder called 'parameter'; 3) executing FASTUV_V1.0.exe. After simulation, the Daily surface solar UV radiation in certain time and locations would be calculated in a file named

'Daily_output.txt'. It should be stated that the 'MyAppInstaller_web.exe' in file folder namely 'UV_Calculation_model\for_redistribution' should be executed if the MATLAB version is not compatible with FASTUV_V1.0.

6. Conclusion

A novel efficient broadband model for estimating surface Ultraviolet radiation (0.280–0.400 μm) was proposed using sunshine duration measurements and MERRA_2 reanalysis products. Then, the applicability of FASTUV model in modeling surface solar UV radiation were validated using surface solar UV radiation measurements at 29 CERN stations. Finally, the spatial and temporal variations of UV values throughout China were investigated.

The FASTUV model was proved to be an efficient model for predicting surface solar UV radiation at CERN stations with high accuracy and strong robustness. The newly proposed ANN method could effectively calculate the cloud transmittance for UV radiation with higher accuracy than that for QPF method. The estimated UV values by FASTUV model showed high agreement with the estimated UV values by Leckner's spectral model with low deviations. Meanwhile, the newly developed UV model (31.577 s) also run faster than Leckner's spectral model (103.829 s), while ensuring the accuracy of the estimate surface UV radiation. Then, the spatial and temporal variations of UV values over mainland China were discussed in this study. Generally, the surface solar UV radiation gradually decreased from Western China to Eastern China, because of the relatively stronger radiation dumping effects in Eastern China. While, the UV values show a trend of firstly rising and then declining, due to the strong atmospheric extinction effects by abundant water vapor in the air in Southern China and the low yearly mean extraterrestrial radiation in Northern China. In terms of the seasonal variation of UV values, it was higher in summer than that in winter. The Qinghai Tibetan Plateau and the Palmier Plateau has always been the areas with highest UV values, while the Northeastern China is the area with the lowest UV values. Meanwhile, the partial effect of the fluctuation of input parameter on the accuracy of FASTUV model was conducted using sensitivity method. The result indicated that the perturbations of AOD could obviously affect the accuracy of the estimated UV values in FASTUV model. The *ps* and *loz* are also proved to be the relatively unimportant factors for the accuracy of FASTUV model.

Certainly, the FASTUV model should be further validated in other climate zones around the world. Moreover, as described above, the model accuracy of FASTUV model is subjected to some objective factors such as the cloud effect on UV radiation and the relatively coarse resolution of MERRA_2 products. Further work should be conducted to improve the model accuracy of FASTUV model. The FASTUV model has been made into a packing software namely 'FASTUV_V1.0' using MATLAB 2015a, but it needs to be further improved in the future.

CRedit authorship contribution statement

Wenmin Qin: Conceptualization, Data curation, Formal analysis, Funding acquisition, Investigation, Methodology, Software, Writing - original draft, Writing - review & editing. **Lunche Wang:** Formal analysis, Funding acquisition, Investigation, Project administration, Resources, Supervision, Writing - review & editing. **Jing Wei:** Data curation, Methodology, Validation, Writing - review & editing. **Bo Hu:** Data curation, Resources, Supervision. **Xun Liang:** Data curation, Software, Validation, Visualization.

Declaration of competing interest

The authors declare that they have no known competing financial interests or personal relationships that could have appeared to influence the work reported in this paper.

Acknowledgements

This work was financially supported by the National Natural Science Foundation of China (No. 41601044), the Special Fund for Basic Scientific Research of Central Colleges, China University of Geosciences, Wuhan (No. CUG190619, and 009-162301124611), and the 111 Project (grant No. B08030). We would like to thank the China Meteorological Administration (CMA) for providing the meteorological and radiation data.

Appendix A. Supplementary data

Supplementary data to this article can be found online at <https://doi.org/10.1016/j.scitotenv.2020.139513>.

References

- Arola, Antti, 2002. Assessment of four methods to estimate surface UV radiation using satellite data, by comparison with ground measurements from four stations in Europe. *J. Geophys. Res.* 107.
- Babar, Bilal, Graversen, Rune, Boström, Tobias, 2019. Solar radiation estimation at high latitudes: assessment of the CMSAF databases, ASR and ERA5. *Sol. Energy* 182, 397–411.
- Beck, Hylke, Vergopolan, Noemi, Pan, Ming, Levizzani, Vincenzo, van Dijk, Albertijn, Weedon, Grahamp, Brocca, Luca, Pappenberger, Florian, Huffman, Georgej, Wood, Ericf, 2017. Global-scale evaluation of 22 precipitation datasets using gauge observations and hydrological modeling. *Hydrol. Earth Syst. Sci.* 21, 6201–6217.
- Bigelow, Dslusser, Slusser, Jr., Beaubien, Af, Gibson, Jh., 1998. The USDA ultraviolet radiation monitoring program. *B Am. Meteorol. Soc.* 79, 601–616.
- Bird, Richard, 1984. A simple, solar spectral model for direct-normal and diffuse horizontal irradiance. *Sol. Energy* 32, 461–471.
- Bo, Hu, Yue-Si, Wang, Guang-Ren, Liu, 2009. Properties of solar radiation over Chinese arid and semi-arid areas. *Atmos. Ocean. Sci. Lett.* 2, 183–187.
- Booth, Charlesr, Lucas, Timothyb, Morrow, Johnh, Weiler, Csusan, Penhale, Pollya, 1994. The United States National Science Foundation's polar network for monitoring ultraviolet radiation. *Ultraviolet Radiation in Antarctica: Measurements and Biological Effects.* 62, pp. 17–37.
- Cadet, Jean-maurice, Bencherif, Hassan, Portafaix, Thierry, Lamy, Kévin, Nongwane, Katlego, Coetzee, Gerrie, Wright, Caradee, 2017. Comparison of ground-based and satellite-derived solar UV index levels at six south African sites. *Int. J. Environ. Res. Pub. He* 14, 1384.
- Calkins, John, Thordardottir, Thorunn, 1980. The ecological significance of solar UV radiation on aquatic organisms. *Nature* 283, 563.
- Cañada, J., 2003. Relationships between UV (0.290–0.385 μm) and broad band solar radiation hourly values in Valencia and Córdoba, Spain. *Energy* 28, 199–217.
- Dayan, Ad, 1993. Solar and ultraviolet radiation. IARC monographs on the evaluation of carcinogenic risks to humans. Vol 55. *J. Clin. Pathol.* 46, 880.
- Farman, Josephc, Gardiner, Briang, Shanklin, Jonathand, 1985. Large losses of total ozone in Antarctica reveal seasonal ClOx/NOx interaction. *Nature* 315, 207.
- Feister, U., Grasnick, K-h., 1992. Solar UV radiation measurements at Potsdam (52° 22' N, 13° 5' E). *Sol. Energy* 49, 541–548.
- Foyo-Moreno, I., Vida, J., Alados-Arboledas, L., 1999. A simple all weather model to estimate ultraviolet solar radiation (290–385 nm). *J. Appl. Meteorol.* 38, 1020–1026.
- Foyo-Moreno, I., Alados, I., Olmo, Fj., Alados-Arboledas, L., 2003. The influence of cloudiness on UV global irradiance (295–385 nm). *Agric. For. Meteorol.* 120, 101–111.
- Fuka, Danielr, Walter, Mtodd, MacAlister, Charlotte, Degaetano, Arthurt, Steenhuis, Tammos, Easton, Zacharym, 2014. Using the climate forecast system reanalysis as weather input data for watershed models. *Hydrol. Process.* 28, 5613–5623.
- Gueymard, Christian, 1995. SMARTS2: A Simple Model of the Atmospheric Radiative Transfer of Sunshine: Algorithms and Performance Assessment. Florida Solar Energy Center, Cocoa, FL.
- Gueymard, Christiana, 2008. REST2: high-performance solar radiation model for cloudless-sky irradiance, illuminance, and photosynthetically active radiation-validation with a benchmark dataset. *Sol. Energy* 82, 272–285.
- Habte, Aron, Sengupta, Manajit, Gueymard, Christiana, Narasappa, Ranganath, Rosseler, Olivier, Burns, Davidm, 2019. Estimating ultraviolet radiation from global horizontal irradiance. *IEEE J. Photovolt.* 9, 139–146.
- Henderson-Sellers, A., 1993. A factorial assessment of the sensitivity of the BATS land-surface parameterization scheme. *J. Clim.* 6, 227–247.
- Hodges, Ki, Lee, Rw, Bengtsson, L., 2011. A comparison of extratropical cyclones in recent reanalyses ERA-interim, NASA MERRA, NCEP CFSR, and JRA-25. *J. Clim.* 24, 4888–4906.
- Hu, Bo, Wang, Yuesi, Liu, Guangren, 2007. Ultraviolet radiation spatio-temporal characteristics derived from the ground-based measurements taken in China. *Atmos. Environ.* 41, 5707–5718.
- Hu, Bo, Wang, Yuesi, Liu, Guangren, 2010. The characteristics of ultraviolet radiation in arid and semi-arid regions of China. *J. Atmos. Chem.* 67, 141–155.
- Hu, Bo, Wang, Yuesi, Liu, Guangren, 2017. Variation characteristics of ultraviolet radiation derived from measurement and reconstruction in Beijing, China. *Tellus B: Chem. Phys. Meteorol.* 62, 100–108.

- Hutchinson, Michael, Xu, Tingbao, 2004. Anusplin Version 4.2 User Guide. Centre for Resource and Environmental Studies. The Australian National University, Canberra, p. 54.
- Iqbal, Muhammad, 2012. An Introduction to Solar Radiation. Elsevier.
- Kanamitsu, Masao., Ebisuzaki, Wesley., Woollen, Jack., Yang, Shi-keng., Hnilo, Jj., Fiorino, M., Potter, Gl, 2002. Ncep-doe amip-ii reanalysis (r-2). *B Am. Meteorol. Soc.* 83, 1631–1644.
- Kanellis, Evangelisgeorge, 2019. Ultraviolet radiation sensors: a review. *Biophys. Rev.* 11, 895–899.
- Katsambas, Andreas, Varotsos, Costasa, Veziryianni, Georgia, Antoniou, Christina, 1997. Surface solar ultraviolet radiation: a theoretical approach of the SUVR reaching the ground in Athens, Greece. *Environ. Sci. Pollut. R.* 4, 69.
- Krotkov, Na, Bhartia, Pk, Herman, Jr, Fioletov, V., Kerr, J., 1998. Satellite estimation of spectral surface UV irradiance in the presence of tropospheric aerosols: 1. Cloud-free case. *J. Geophys. Res. Atmos.* 103, 8779–8793.
- Krotkov, Na, Herman, Jr, Bhartia, Pk, Fioletov, V., Ahmad, Z., 2001. Satellite estimation of spectral surface UV irradiance: 2. Effects of homogeneous clouds and snow. *J. Geophys. Res. Atmos.* 106, 11743–11759.
- Lamy, Kevin, Portafaix, Thierry, Brogniez, Colette, Godin-Beckmann, Sophie, Bencherif, Hassan, Morel, Beatrice, Pazmino, Andrea, Metzger, Jeanmarc, Aurio, Frederique, Deroo, Christine, 2018. Ultraviolet radiation modelling from ground-based and satellite measurements on Reunion Island, southern tropics. *Atmos. Chem. Phys.* 18, 227–246.
- Láska, K., Budík, L., Budíková, M., Prošek, P., 2011. Method of estimating solar UV radiation in high-latitude locations based on satellite ozone retrieval with an improved algorithm. *Int. J. Remote Sens.* 32, 3165–3177.
- Lean, Judithl, Rottman, Garyj, Kyle, Hlee, Woods, Thomasn, Hickey, Johnr, Puga, Lawrencee, 1997. Detection and parameterization of variations in solar mid-and near-ultraviolet radiation (200–400 nm). *J. Geophys. Res. Atmos.* 102, 29939–29956.
- Leckner, Bo, 1978. The spectral distribution of solar radiation at the earth's surface—elements of a model. *Sol. Energy* 20, 143–150.
- Liu, H., Hu, B., Zhang, L., Zhao, Xj., Shang, Kz., Wang, Ys., Wang, J., 2017. Ultraviolet radiation over China: spatial distribution and trends. *Renew. Sust. Energ. Rev.* 76, 1371–1383.
- Madronich, Sasha, de Grujil, Frankr, 1993. Skin cancer and UV radiation. *Nature* 366, 23.
- Madronich, Sasha, McKenzie, Richardl, Björn, Larso, Caldwell, Martynm, 1998. Changes in biologically active ultraviolet radiation reaching the Earth's surface. *J. Photochem. Photobiol. B Biol.* 46, 5–19.
- McKenzie, Rl, Paulin, Kj, Bodeker, Ge, Liley, Jb, Sturman, Ap, 1998. Cloud cover measured by satellite and from the ground: relationship to UV radiation at the surface. *Int. J. Remote Sens.* 19, 2969–2985.
- Nunez, Manuel, Forgan, Bruce, Roy, Colin, 1994. Estimating ultraviolet radiation at the earth's surface. *Int. J. Biometeorol.* 38, 5–17.
- Peng, Simao, Du, Qingsyun, Wang, Lunche, Lin, Aiwen, Hu, Bo, 2015. Long-term variations of ultraviolet radiation in Tibetan Plateau from observation and estimation. *Int. J. Climatol.* 35, 1245–1253.
- Prescott, Ja, 1940. Evaporation from a water surface in relation to solar radiation. *Trans. Roy. Soc. S. Aust.* 46, 114–118.
- Qin, Wenmin, Wang, Lunche, Lin, Aiwen, Zhang, Ming, Xia, Xiangao, Hu, Bo, Zigeng, Niu, 2018a. Comparison of deterministic and data-driven models for solar radiation estimation in china. *Renew. Sust. Energ. Rev.* 81, 579–594.
- Qin, Wenmin, Liu, Ying, Wang, Lunche, Lin, Aiwen, Xia, Xiangao, Che, Huizheng, Muhammad Bilal, Zhang, Ming, 2018b. Characteristic and driving factors of aerosol optical depth over mainland china during 1980–2017. *Remote. Sens.-Basel* 10, 1064.
- Qin, Wenmin, Wang, Lunche, Lin, Aiwen, Zhang, Ming, Bilal, Muhammad, 2018c. Improving the estimation of daily aerosol optical depth and aerosol radiative effect using an optimized artificial neural network. *Remote. Sens.-Basel* 10, 1022.
- Qin, Wenmin, Wang, Lunche, Zhang, Ming, Niu, Zigeng, Luo, Ming, Lin, Aiwen, Hu, Bo, 2019. First effort at constructing a high-density photosynthetically active radiation dataset during 1961–2014 in china. *J. Climate* 32, 2761–2780.
- Sabbagh, J., Wong, J., 2000. Evaluation of a sky/cloud formula for estimating UV-B irradiance under cloudy skies. *J. Geophys. Res. Atmos.* 105, 29685–29691.
- Singh, Sachidanand, Lodhi, Neeleshk, Mishra, Amitkumar, Jose, Sandhya, Kumar, Snaresh, Kotnala, Rk, 2018. Assessment of satellite-retrieved surface UVA and UVB radiation by comparison with ground-measurements and trends over Mega-city Delhi. *Atmos. Environ.* 188, 60–70.
- Tang, Wenjun, Yang, Kun, Qin, Jun, Min, Niu, Xiaolei, 2018. First effort for constructing a direct solar radiation data set in China for solar energy applications. *J. Geophys. Res. Atmos.* 123, 1724–1734.
- Tanskanen, Aapo, Krotkov, Nickolaya, Herman, Jayr, Arola, Antti, 2006. Surface ultraviolet irradiance from OMI. *IEEE T Geosci. Remote* 44, 1267–1271.
- Verdebout, Jean, 2000. A method to generate surface UV radiation maps over Europe using GOME, Meteosat, and ancillary geophysical data. *J. Geophys. Res. Atmos.* 105, 5049–5058.
- Wang, Lunche, Gong, Wei, Feng, Lan, Hu, Bo, 2015. UV variability in an arid region of Northwest China from measurements and reconstructions. *Int. J. Climatol.* 35, 1938–1947.
- Wang, Mengmeng, He, Guojin, Zhang, Zhaoming, Wang, Guizhou, Zhang, Zhengjia, Cao, Xiaojie, Wu, Zhijie, Liu, Xiuguo, 2017. Comparison of spatial interpolation and regression analysis models for an estimation of monthly near surface air temperature in china. *Remote. Sens.-Basel* 9, 1278.
- Wei, Jing, Huang, Wei, Li, Zhanqing, Xue Wenhao, Cribb Maureen, 2019a. Estimating 1-km-resolution pm2.5 concentrations across china using the space-time random forest approach. *Remote. Sens. Environ.* 231, 111221.
- Wei, Jing, Li, Zhanqing, Guo, Jianping, Sun, Lin, Cribb Maureen, 2019b. Satellite-derived 1-km-resolution pm1 concentrations from 2014 to 2018 across china. *Environ. Sci. Technol.* 53, 13265–13274.
- Williamson, Craige., Zepp, Richardg., Lucas, Robynm., Madronich, Sasha., Austin, Amyt., Ballare, Carlosl., Norval, Mary., Sulzberger, Barbara., Bais, Alkiividisf., McKenzie, Richardl, 2014. Solar ultraviolet radiation in a changing climate. *Nat. Clim. Chang.* 4, 434–441.
- Yang, Kun, He, Jie, Tang, Wenjun, Qin, Jun, Cheng, Charlesck, 2010. On downward short-wave and longwave radiations over high altitude regions: observation and modeling in the Tibetan Plateau. *Agric. For. Meteorol.* 150, 38–46.